Sensors and Actuators B 239 (2017) 253–261

Contents lists available at ScienceDirect

Sensors and Actuators B: Chemical

journal homepage: www.elsevier.com/locate/snb

Gas sensor properties of Ag- and Pd-decorated SnO micro-disks to NO_2, H_2 and CO: Catalyst enhanced sensor response and selectivity

Martin S. Barbosa[a], Pedro H. Suman[a,b], Jae J. Kim[b], Harry L. Tuller[b], José A. Varela[a], Marcelo O. Orlandi[a,*]

[a] Department of Physical-Chemistry, São Paulo State University, Araraquara, SP, 14800-900, Brazil
[b] Department of Materials Science and Engineering, Massachusetts Institute of Technology, Cambridge, MA, 02139, USA

ARTICLE INFO

Article history:
Received 4 April 2016
Received in revised form 27 July 2016
Accepted 27 July 2016
Available online 27 July 2016

Keywords:
Gas sensors
SnO
Catalyst
Impedance spectroscopy
Sensitization

ABSTRACT

The gas sensor response of tin monoxide micro-disks, functionalized with noble metal nanoparticles (Pd and Ag), to NO_2, H_2 and CO were studied by monitoring changes in their resistance upon exposure to the various gases. The tin monoxide, with unusually low Sn oxidation state, was synthetized by carbothermal reduction. Surface modification by Pd and Ag catalysts was achieved by coating the micro-disks by metallic nanoparticle dispersions, prepared by the polyol reduction process, followed by thermal treatment. SEM and TEM analysis showed nanoparticles to be well-dispersed over the SnO surfaces. The decorated SnO micro-disks exhibited high sensor response to reducing gases such as H_2 and CO. On the other hand, the catalytic particles tended to reduce the sensor response to oxidizing gases such as NO_2. The catalytic activity of Pd nanoparticles was tied to chemical sensitization while that of Ag nanoparticles to electronic sensitization. Impedance spectroscopy enabled deconvolution of different contributions to the sensor response with only the Ag-decorated specimens exhibiting two RC time constants. Thus, in contrast to undecorated and Pd-decorated specimens, nearly 80% of Ag modified SnO's response to H_2 was controlled by changes in the interface between particles and disks. Sensor response to H_2 was optimal at higher temperatures (300 °C), NO_2 at 200 °C while that for Pd-decorated materials; maximum sensor response to CO was observed at lower temperatures (under 150 °C), where CO absorption by metal nanoparticles is favored.

1. Introduction

Growing concerns about the impact of gas emissions on health and the environment have driven the search for ever faster responding and more highly sensitive gas sensors with a focus on the detection of flammable (H_2, ethanol, hydrocarbons) and toxic (H_2S, CO, NO_2, Cl_2) gases at low levels (ppm or ppb) and in the presence of interferents. Semiconductor metal oxide (SMO) based sensors, whose resistivity is modulated by the adsorption/desorption of a designated chemical species on the surface of the SMOs, have received a great deal of attention, given good performance coupled with low cost materials and simple device design [1]. Performance improvements can be achieved by taking advantage of high surface area and/or quantum mechanical effects for appropriately engineered SMOs on the micro- and nano-scale [2].

Further enhancements in performance can be achieved by addition of other phases to the metal oxide matrix by promoting increased physical and chemical interactions between the gas and the host material surface [3]. Such surface modification, known as decoration or functionalization, may include the addition of noble metal (Au, Ag, Pt, Pd) nanoparticles (NPs) that act as catalysts, influencing the adsorption processes (chemical sensitization) and/or the position of surface energy levels (electronic sensitization) [4]. The decoration of SMOs with noble metal nanoparticles has led to large increases in sensor response in many different oxide matrices [5–8]. The best results are commonly observed for small-sized particles (<100 nm) in lower concentrations (0.1–10 wt%), and high surface dispersion, thereby promoting catalytic activity without compromising the host material's function [9].

Tin oxide based materials are among the most used semiconductors for gas sensor technology given their high thermal and chemical stability and reasonable cost [10]. While tin dioxide (SnO_2), with various morphologies (porous thick and thin films

* Corresponding author at: Department of Physical-Chemistry, São Paulo State University – UNESP, Rua Francisco Degni 55, Quitandinha, P.O. Box 355, CEP: 14800-900, Araraquara, São Paulo, Brazil.
E-mail address: orlandi@iq.unesp.br (M.O. Orlandi).

http://dx.doi.org/10.1016/j.snb.2016.07.157
0925-4005/

and 1-D nanowires), is the most widely studied gas sensor material, recent results by the authors have shown that tin monoxide (SnO) can also exhibit an exceptional sensor response [11] even higher than the SnO_2-based sensors [12]. Because of questions regarding its thermal and chemical stability (the disproportionation reaction of SnO to SnO_2 and Sn^0 occurs at ~400 °C [13]), there are very few studies relating to SnO based sensors, even without surface modification. In this work, we report the surface decoration of SnO micro-disks with noble metals nanoparticles (Ag and Pd) and their impact on the detection of H_2, NO_2 and CO.

2. Materials and methods

The synthesis of SnO disk-like structures was conducted via the carbothermal reduction method. The precursors used were SnO_2 (Sigma-Aldrich, 99.9% purity) and carbon black (Union Carbide, >99% purity) powders. Both powders were mixed together in the molar ratio of 1.5:1 (SnO_2:C) in an agate mortar, following which the mixture was inserted into a tubular furnace at 1135 °C in the presence of a N_2 flow of 80 sccm for 75 min in order to grow SnO materials under optimized conditions, as detailed in our previous work [14]. After synthesis, a dark material was retrieved from the alumina tube walls. Both SnO micro-disks and nanobelts were simultaneously obtained and subsequently separated by sedimentation in isopropyl alcohol and then dried at 70 °C.

The catalytic nanoparticle dispersions were prepared by the polyol reduction method [15] with specific conditions for each metal. All synthesis took place in a three-necked round flask, partially filled with ethylene glycol, using magnetic stirring. For the synthesis of Pd nanoparticles, two solutions were simultaneously added to 5 mL of ethylene glycol (at 120 °C) at a rate of 45 mL h^{-1}. The first solution was composed of 1.6 mL of $PdCl_2$ (Sigma-Aldrich, 0.053 g mL^{-1} in a 0.17 g mL^{-1} HCl aqueous solution) and the second one was a solution of 0.08 g polyvinylpyrrolidone (PVP, Sigma-Aldrich, average Mw 34,000 g/mol) dissolved in 5 mL of ethylene glycol. Another solution containing 6.5 mL of NaOH (0.007 g mL^{-1}) was added in order to facilitate the reduction reaction [16]. The mixture was heated to 120 °C for 9 h.

For the Ag nanoparticles, two solutions were simultaneously added to 5 mL of ethylene glycol (at 140 °C) at a rate of 45 mL h^{-1}. The first solution was composed of 0.48 g of $AgNO_3$ (Sigma-Aldrich, >99% purity) dissolved in 3 mL of ethylene glycol, and the second one was composed of 0.10 g of PVP and 0.0004 g of NaCl (added to control the size of the particles [17]) dissolved in 3 mL of ethylene glycol. To obtain the desired nanoparticles, temperature and agitation were maintained at 150 °C for 40 h.

The decoration process of the SnO micro-disk surfaces with the metallic nanoparticles was achieved by a *self-assembly* process [18] by mixing 0.05 g of SnO micro-disks with sufficient amount of NP dispersions to obtain an approximately 1 wt% loading. The mixture was further dispersed using an ultrasonic cleaner, dried at 80 °C and annealed at 350 °C for 4 h in air in order to ensure thermal stability of SnO host material. The morphological characteristics of the metallic nanoparticles, the pristine SnO structures and the NP-decorated SnO structures were characterized by field-emission scanning electron microscopy (FE-SEM; JEOL, JSM-7500F) equipped with X-ray energy dispersive spectroscopy (EDS). Further, phase and crystallinity of materials were studied by transmission electron microscopy (TEM; Philips, CM200) operated at 200 kV.

In order to perform FE-SEM analysis, the materials were initially dispersed with the aid of an ultrasonic cleaner. A few drops of each solution (either the pristine SnO structures, metallic nanoparticles or NP-decorated SnO structures) were dropped onto conductive Si substrates. For the metallic nanoparticles, the same thermal treatment was carried out as that one used in the decoration step (annealing at 350 °C for 4 h in air). This treatment was necessary to evaporate any residual solvent and to decompose any remaining PVP from the synthesis process. Specimens for TEM analysis were prepared by dripping droplets of solution onto copper grids, followed by drying at room temperature.

The chemical composition of the material surfaces was analyzed by X-ray Photoelectron Spectroscopy (XPS) using a commercial spectroscope (UNI-SPECS UHV SYSTEM) operating with an Mg *K*α X-ray source producing photons with energy of 1253.6 eV and working at a vacuum pressure of 5×10^{-7} Pa. The spectra were decomposed using a Voigtian function, utilizing a combination of Gaussian and Lorentzian components. Binding energy scale of the XPS spectra was calibrated by setting the peak energy of adventitious carbon (C 1s peak) to 285 eV. Gas sensing devices were fabricated by ultrasonically dispersing the as-prepared materials (pristine and Pd- and Ag-decorated SnO micro-disks) in isopropyl alcohol and drop-casting the solutions onto alumina substrates patterned with platinum interdigitated electrodes arrays (100 μm Pt fingers spaced 200 μm apart). The devices were then heated to 100 °C to remove the solvent. Gas sensing measurements were conducted by monitoring changes in electrical resistance in the presence of different atmospheres with the aid of an HP34970A data acquisition unit operating with a DC voltage of 100 mV. The tested gas mixtures were composed of synthetic dry air (baseline atmosphere) and different analyte gases (NO_2, H_2 and CO) in various concentrations, ranging from 1 ppm to 1000 ppm, controlled by mass flowmeters (MKS). Working temperatures in the range of 100 °C to 350 °C were used. Before each series of measurements, the sensors were exposed to synthetic dry air for 12 h to stabilize the baseline resistance. The gas sensing properties were expressed as a function of sensor response, defined either as the ratio between the electrical resistance in the baseline atmosphere and the electrical resistance in the presence of the analyte gases (R_0/R_{gas}) for the reducing gases (CO and H_2) or as (R_{gas}/R_0) for the oxidizing gas (NO_2). The same devices were also characterized by impedance spectroscopy (IS) using a Modulab system (Solartron Analytical), with a 0.1 V amplitude signal in the frequency range between 10^{-1} Hz and 10^6 Hz.

3. Results and discussion

3.1. Morphological and structural characterization

The morphological and structural characterizations of pristine SnO micro-disks before the decoration step (without noble metal nanoparticles) were previously reported [11,14] and showed that the disks are single-crystalline with diameters ranging from 0.1 μm to 10 μm. Fig. 1 presents electron microcopy (EM) images of noble metal nanoparticles (NPs) obtained by the polyol synthesis method. The SEM image (Fig. 1a) indicates that the Pd NPs are agglomerated, but TEM characterization shows that is possible to disperse them by ultrasonication. High resolution TEM (HRTEM) and selected area electron diffraction (SAED) images of the nanoparticles are illustrated in Fig. 1b. The Pd nanoparticles were cubic (JCPDS card #46-1043) and could be identified by indexing the planar distances observed on the SAED pattern. Moreover, HRTEM image of the Pd NPs shows that each nanoparticle is single-crystalline. The SEM and TEM analyses of the Pd show it to be composed of nanoparticles with average diameter below 15 nm as shown in the histogram in Fig. 1c. By SEM imaging in Fig. 1d it is possible to observe that the Ag synthesis yielded well-dispersed particles with bi-modal size distribution, with particle diameter ranging from 4 nm up to 200 nm. The size distribution histogram for the smaller particles is shown in Fig. 1f with mean diameter of 12 nm. Fig. 1e shows HRTEM and SAED images of the Ag nanoparticles. All of the rings in the SAED pattern

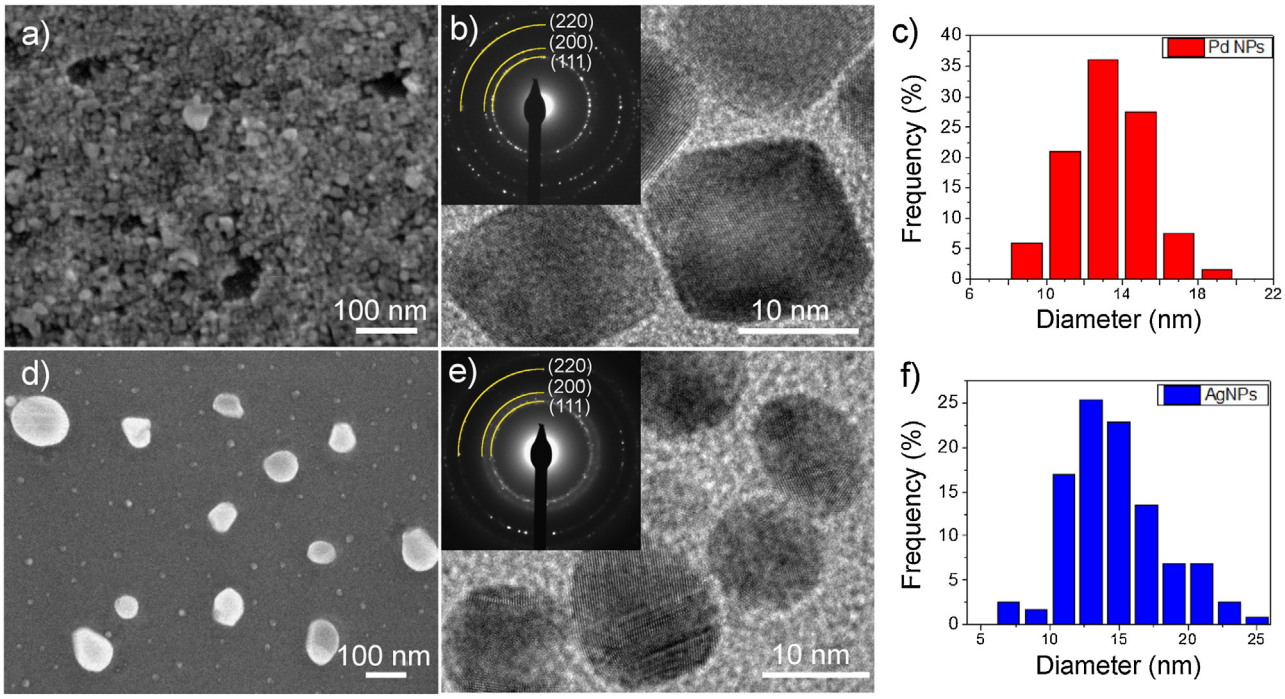

Fig. 1. Metallic NPs morphological characterization. Pd: (a) FE-SEM image, (b) HRTEM image with SAED and (c) particle size distribution. Ag: (d) FE-SEM image, (e) HRTEM image with SAED and (f) particle size distribution.

can be indexed by the cubic structure of Ag metallic phase (JCPDS card #65-2871). Moreover, each Ag NP presents a single-crystalline character, as observed from the HRTEM image.

The EM images of the Pd-decorated SnO micro-disks are shown in Fig. 2. The Pd nanoparticles are dispersed in small clusters on the surface of the SnO structures, indicating successful decoration of the micro-disks (Fig. 2a). The interplanar distances observed by HRTEM (Fig. 2b) are (0.22 ± 0.1) nm for the NPs and (0.27 ± 0.1) nm for the SnO micro-disks, which are related to the (111) and (110) planes of each structure. This reveals that after decoration, the NPs are still in their metallic phase (important for catalytic activity), while SnO remains in the tetragonal phase (JCPDS card # 6-0395).

Fig. 3 shows EM characterization of Ag-decorated SnO micro-disks. Again, it is possible to observe from Fig. 3a a good dispersion of the Ag NPs on the surface of the disks, with only the smaller particles decorating the SnO structures, which can be favorable for enhanced catalytic activity. HRTEM image (Fig. 3b) revealed an interplanar distance of (0.24 ± 0.1) nm for the Ag NPs, which are related to the (111) planes of cubic structure of the metal, as observed by SAED pattern of this material in Fig. 1e, and an interplanar distance of (0.37 ± 0.1) nm for the SnO micro-disks, related to the (100) planes of the SnO tetragonal structure. It means that SnO remains in the tetragonal phase after the decoration process by silver nanoparticles. For both catalysts used in this work, self-assembly treatments promote the deposition of particles while maintaining their metallic character, without compromising the crystalline phase of the SnO host material.

To investigate the chemical composition, bonding and oxidation state of the materials, X-ray photoelectron spectroscopy (XPS) analyses were performed on the pristine and decorated materials. Fig. 4a exhibits the survey scan of the pristine (black line), Pd (red line) and Ag (blue line) decorated structures. Results from the elemental quantification exhibited an external surface ratio between oxygen and tin of 1.4 (O/Sn) for all samples. This result is in agreement with previous XPS analysis performed on SnO materials [19], which indicated that an oxygen rich surface (2–3 nm thick) may

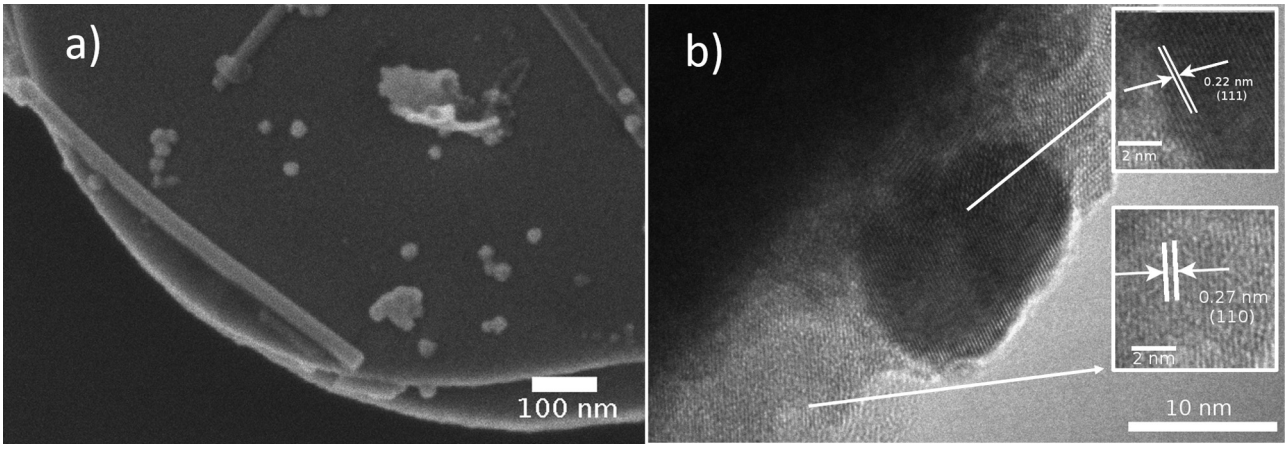

Fig. 2. Pd-decorated SnO structures: EM images of Pd-decorated SnO disk-like structures (a) FE-SEM and (b) HRTEM image of a SnO/Pd interface with planar distance indexing.

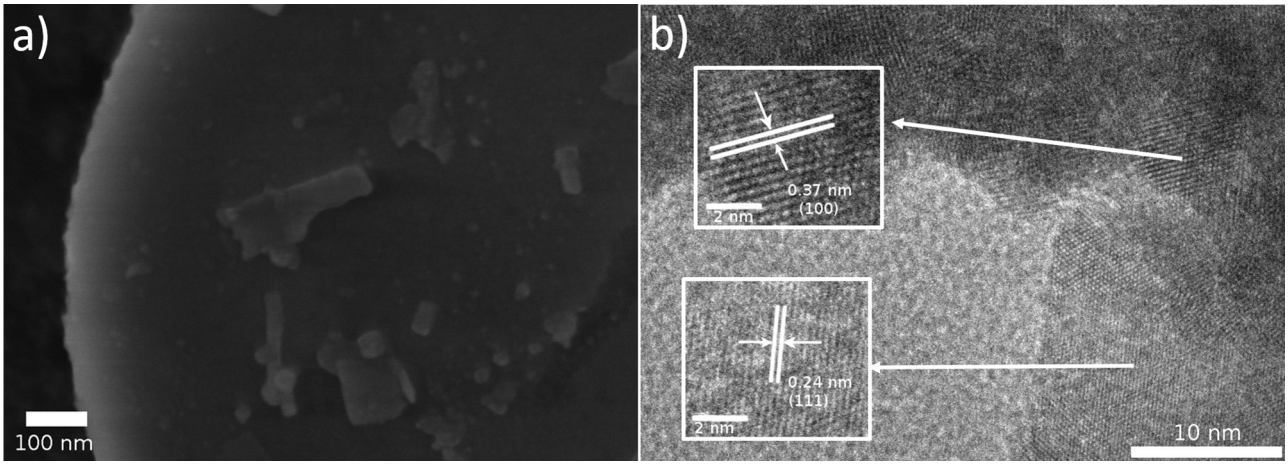

Fig. 3. Ag-decorated SnO structures: EM images of Ag-decorated SnO disk-like structures (a) FE-SEM and (b) HRTEM image of a SnO/Ag interface with planar distance indexing.

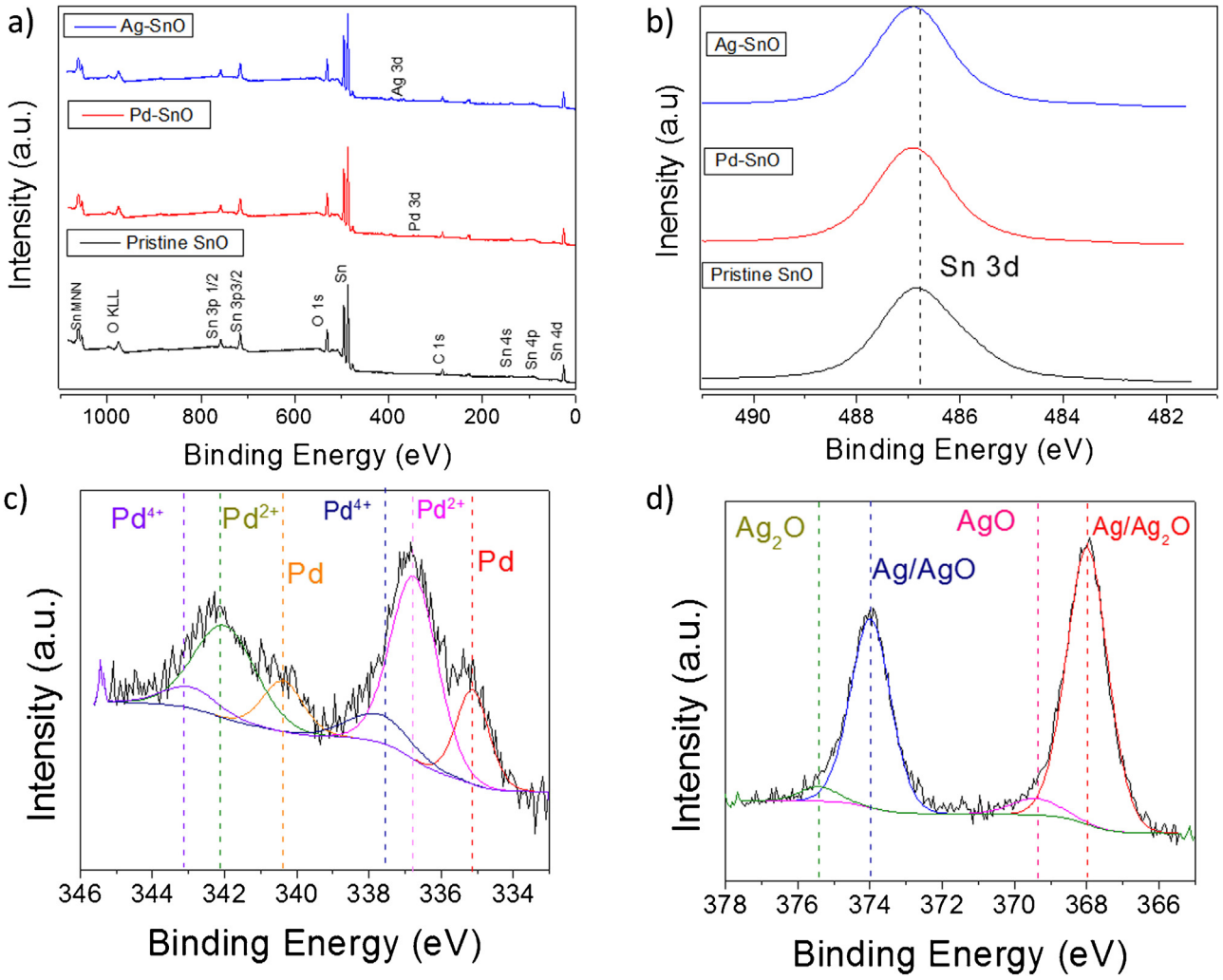

Fig. 4. XPS analysis of the pristine and decorated SnO materials: (a) Survey scan spectrum and (b) high resolution spectra of the Sn 3d peak, obtained on the three different materials. (c) High resolution spectra of the Pd 3d peaks and (d) Ag 3d peaks. (For interpretation of the references to colour in the text, the reader is referred to the web version of this article.)

be present on the surface of SnO resulting from synthesis conditions. X-ray diffraction and *in situ* X-ray absorption near edge spectroscopy (XANES) results presented by our group in previous work [11], alongside the HRTEM and SAED analyses, indicate that there is no evidence for a distinct SnO_2 phase at the surface. Elemental analysis performed on the decorated structures also indicated the atomic fraction of metallic NPs to be 0.4% for Pd (0.7% in weight percentage) and 0.9% for Ag (1.3% in weight percentage), indicat-

ing that the decoration was successfully achieved on levels close to the targeted 1% in weight percentage. Fig. 4b shows the high resolution spectra of the Sn 3d peak for the three different materials. The peak is composed by both Sn^{4+} and Sn^{2+} chemical shifts, and it is not possible to distinguish their oxidation state and proportion based solely on this information. Fig. 4c shows the high resolution spectra of the Pd 3d peak for the Pd-decorated materials. One observes peaks corresponding to Pd in multiples states of oxidation. The $3d_{5/2}$ peaks at 336.9 eV and 337.5 eV can be attributed to the oxides PdO (Pd^{2+}) and PdO_2 (Pd^{4+}), respectively. A peak at 335.7 eV was also observed, indicating that the metallic state is also present (Pd^0), as observed by TEM. A second set of peaks corresponding to the $3d_{3/2}$ levels associated with Pd^{2+} at 342 eV and 337 eV was observed with a separation of approximately 5 eV, in agreement with the spin-orbit doublet separation value that can be found in the literature (5.3 eV) [20]. Fig. 4d shows the high resolution spectra of the Ag $3d_{5/2}$ peak for the Ag-decorated materials with peaks corresponding to Ag, Ag_2O and AgO at 368.3, 367.9, and 367.3 eV, respectively. Due to the closeness of the binding energy between Ag and AgO, their peaks could not be fully resolved, but these results nevertheless indicate that Ag exists in more than one oxidation state [21].

3.2. Gas sensing characterization

Gas sensor measurements were performed simultaneously for the pristine and noble metal decorated samples upon exposure to either H_2, NO_2 or CO. Fig. 5a shows the sensor response as a function of time for an exposure program of periodic H_2 pulses (20 min long) with concentrations ranging from 10 to 1000 ppm, for pristine and NP-decorated SnO disk-like structures at the working temperature of 300 °C. Sensor responses for all materials, corresponding to measurements performed at 1000 ppm H_2 as a function of the operating temperature, are shown in Fig. 5b. The Pd-decorated SnO microdisks (red curve) clearly exhibits higher sensor response at 300 °C compared to the pristine SnO structures (black curve). This difference was greater as the H_2 concentration increased. One should also notice that the Pd-decorated SnO sensor exhibited an overshoot effect, i.e. the sensor response just after exposure to the analyte gas was highest followed by a signal decay up to the end of the gas pulse. Also of interest is the linear dependence of the Pd-decorated sample sensor response with temperatures between 150–300 °C, above which an additional increase in temperature does not lead to further increases in sensor response (Fig. 5b).

To clarify the catalytic effect promoted by Pd NPs on SnO surface, it is important to investigate the nature of the H_2 interaction with the surfaces of the SnO_x based sensors. The SnO_x surface is proposed to be covered with either atomic (O^-, at high temperatures) or molecular (O_2^-, at low temperatures) species, interacting with lone pair electrons in oxygen rich atmospheres (e.g., synthetic dry air) at temperatures under 400 °C. When H_2 is introduced, it reacts with the oxygen species, with the release of electrons responsible for decreasing the material's resistance, based on the following reactions:

Scheme 1. Proposed model for H_2 interaction with O species over SnO_x surface.

$$2H_{2(g)} + O^-_{2(SnO)} \rightarrow 2H_2O_{(g)} + e^-_{(SnO)} \quad (1)$$

$$H_{2(g)} + O^-_{(SnO)} \rightarrow H_2O_{(g)} + e^-_{(SnO)} \quad (2)$$

When Pd NPs are present on the material's surface, an additional catalytic step is introduced, as Pd can react with H_2, by breaking the H—H bond and bind directly with atomic H, in a process known as *split-over* [22]. Following that step, Pd-bound H migrates to the surface of SnO to react with the adsorbed oxygen species (*spillover*), to further promote a free electron [23]:

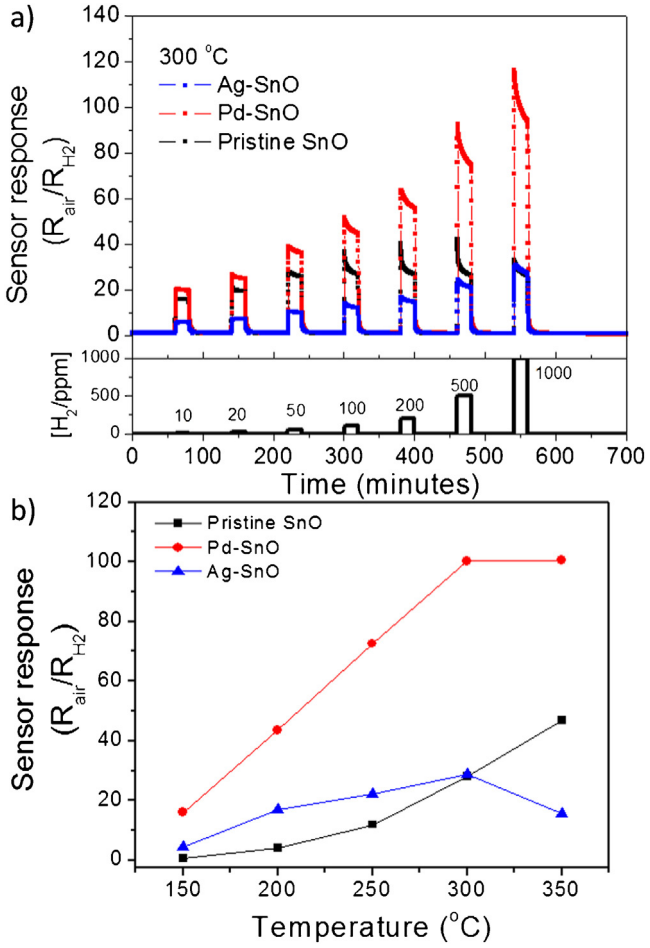

Fig. 5. (a) Sensor response obtained for pristine and Pd- and Ag-decorated SnO disk-like structures at 300 °C for a series of H_2 pulses with concentrations ranging from 10 to 1000 ppm. (b) Maximum sensor response measured for 1000 ppm H_2 exposure, plotted as a function of operating temperature for the pristine and decorated SnO disk-like structures. (For interpretation of the references to colour in the text legend, the reader is referred to the web version of this article.)

Scheme 2. Proposed model for Pd sensitization of the H_2 interaction with O species over Pd-decorated SnO_x surface.

$$H_{2(g)} \xrightarrow{Pd} 2H_{(Pd)}\,(split-over) \quad (3)$$

$$4H_{(Pd)} + O^-_{2(SnO)} \rightarrow 2H_2O_{(g)} + e^-_{(SnO)}\,(spillover) \quad (4)$$

$$2H_{(Pd)} + O^-_{(SnO)} \rightarrow H_2O_{(g)} + e^-_{(SnO)}\,(spillover) \quad (5)$$

As adsorption is facilitated by the introduction of this step to the kinetic process, a chemical sensitization phenomenon is present, increasing the material's sensor response to H_2, as has been reported for SnO_2 based sensors [24]. Thus an increase in sensor response was expected, as observed for the sensors based on Pd-decorated SnO disks when exposed to hydrogen.

Ag-decorated structures (blue curve, Fig. 5b) also exhibited an increase in sensor response over that of the pristine specimen in the presence of 1000 ppm H_2 for measurements performed at temperatures of 250 °C and below but not as high as for Pd-decorated device. Interestingly, the sensor response of Ag-decorated SnO began to drop below that of the pristine material from 300 °C (except for 1000 ppm H_2 at 300 °C). H_2 sensors, based on Ag-decorated SnO_2 materials, have been reported to show an enhanced electronic effect, due to the oxidation of Ag nanoparticles that sets a redox

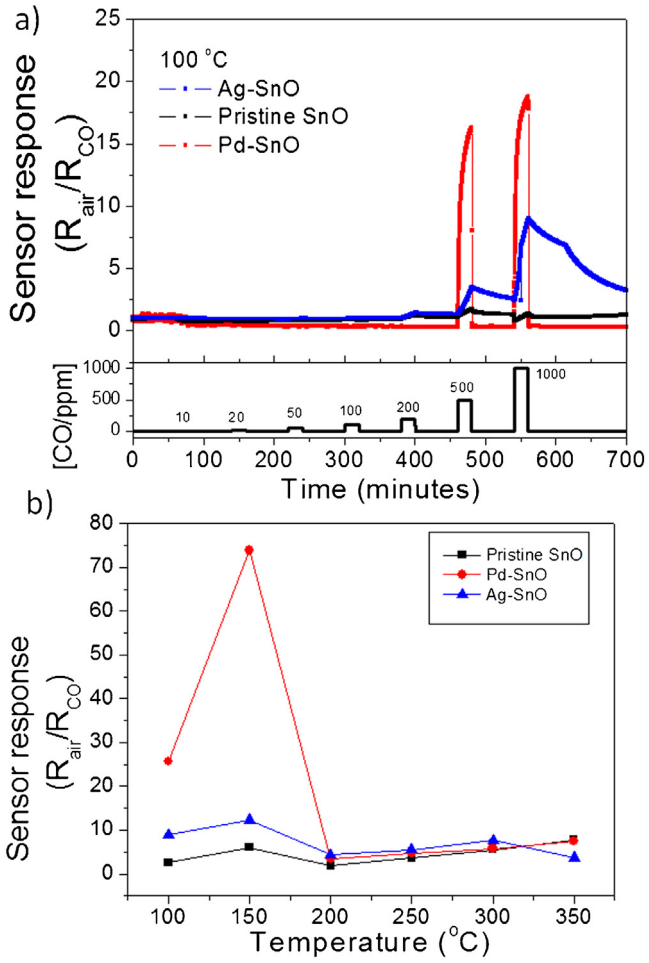

Fig. 6. (a) Sensor response to CO exposure at 100 °C for a series of CO pulses with concentrations ranging from 10 to 1000 ppm for the pristine and decorated SnO disk-like structures. (b) Maximum sensor response measured for 1000 ppm CO exposure as a function of operating temperature for the pristine and decorated SnO disk-like structures.

pair (Ag^+/Ag^0) equilibrium in oxygen rich atmospheres [25]. This creates an electron-depleted region around the Ag NPs, and when the material is exposed to a reducing gas (such as H_2), the shift of the equilibrium to the reduced state promotes the pinning of the oxide's Fermi energy with the metal work function, resulting in a greater increase in conductivity [25]. A similar electronic sensitization effect seems to be occurring (the pristine and Ag-decorated materials have different conductivities and sensor response), but one must keep in mind that SnO and SnO_2 have different ionization potentials, i.e, 4.79 eV for SnO_2 [3] and 5.8 eV for SnO [26]. This difference can affect the junction barriers promoted by either Ag or AgO species, depending on the oxidative/reductive characteristics of the atmosphere. Further, studies on the activation energies of the decorated materials are being conducted to understand the extent of these electronic sensitization effects on SnO sensors.

The pristine and decorated SnO structures were also characterized for exposure to CO using the same exposure cycle used during the H_2 characterization. Fig. 6a shows the sensor response as function of time for measurements performed at 100 °C and Fig. 6b shows the sensor response obtained for measurements at 1000 ppm as function of operating temperature. Pd-decorated SnO structures exhibited a large increase in sensor response at low working temperatures (150 °C) and at large concentrations (over 500 ppm). This follows from the fact that group 10 (Pd, Pt, Cr) metals are known to adsorb CO at temperatures below 150 °C, due to the π −backbonding interaction [27] between the filled *d* orbitals of the metal and the empty π^* molecular orbitals of CO. The SnO_x sensor response for CO detection relies on the oxidation of CO to CO_2 by reaction of the CO with adsorbed oxygen species. This reaction is further catalyzed by the adsorption of CO on the metallic NPs [28,29], and is attributed to the chemical sensitization model as:

Scheme 3. Proposed model for chemical sensitization promoted by group 10 metals nanoparticles on the CO interaction with O species over SnO_x surface.

$$CO \xrightarrow{M} CO(M) \quad (6)$$

$$2CO(M) + O_2^- \rightarrow 2CO_2 + e^- \quad (7)$$

$$CO(M) + O^- \rightarrow CO_2 + e^- \quad (8)$$

For the measurements performed at 150 °C, the Pd-decorated structures exhibited a strong response to CO at a concentration of 1000 ppm (approximately 75), but very low response (under 5) for any other concentration (not shown here). At temperatures higher than 150 °C, the Pd-CO interaction is not favored [30] and the catalytic effect is no longer present. For the measurements performed under these conditions, no significant difference in the sensor response of undecorated and decorated structures was observed.

The Ag-decorated SnO structures exhibited a small increase in CO sensor response for all measurements below 350 °C. However, just as observed for the pristine structures, the sensor response was never higher than 15. This weak effect was previously observed for Ag-decorated SnO_2 sensors, and was attributed to the Ag^+/Ag^0 redox equilibrium working as electron-acceptors [31].

To test Pd and Ag decoration effects on sensor response to oxidizing gases, the sensor based on SnO structures were exposed to NO_2 using a similar program as used for the reducing gases, but in concentrations ranging from 1 ppm to 100 ppm. Fig. 7a shows the sensor response following a series of NO_2 pulses for measurements performed at 250 °C, while Fig. 7b shows the sensor response as function of operating temperature for the maximum level of NO_2 exposure (100 ppm). Since the electrical resistance of the decorated samples for temperatures below 250 °C was above the upper limit that the instrumentation was capable of measuring, these samples were only characterized for 250 and 300 °C. As shown in Fig. 7, the pristine SnO structures have the highest sensor response for all conditions of gas concentration and temperature, indicating that the metal NPs act to inhibit the interaction of the sensor with NO_2. Thus, opposite to the response of the decorated SnO sensor to H_2 and CO, the catalysts had a negative influence on sensor response. This is consistent with our previous observation that the high sensor response of SnO to NO_2 is due to the electron lone pairs associated with divalent Sn [11], resulting in a Giant Chemo-Resistance (GCR) effect. The electronic effect, introduced by the metallic NPs, via Schottky barrier formation, leading to electron depleted regions associated with redox pairs (such as Ag^+/Ag^0), make free electrons less available for interaction with NO_2, resulting in the observed decrease in sensor response [32].

The consequence of sensor response enhancement for reducing gases due to catalytic effects, and suppression for NO_2 detection on the sensor selectivity can be observed in Fig. 8. The sensor response observed following exposure to the various gases at 100 ppm concentration shows the high selectivity of the pristine SnO structure to NO_2 at 200 °C. At the same time, the Pd-decorated SnO structures at 300 °C exhibit strong selectivity for H_2 compared to the pristine and Ag-decorated samples. Thus Pd-decorated SnO structures show great potential for detecting reducing gases with high sensor response and with strong selectivity particularly to H_2, while undecorated SnO specimens remain highly selective to NO_2.

To further investigate the mechanisms behind the observed catalytic effects, complementary impedance spectroscopy (IS)

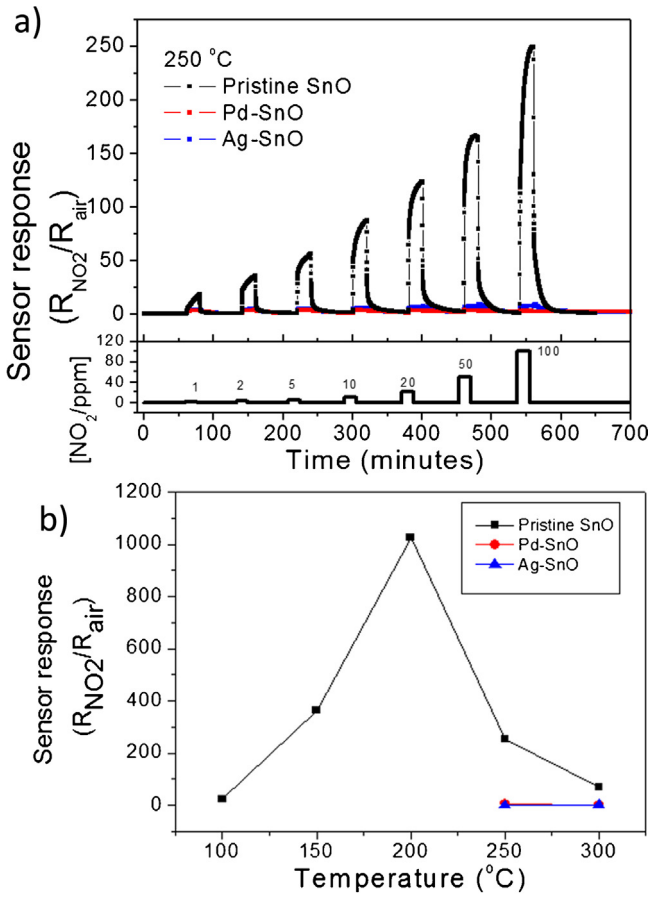

Fig. 7. (a) Sensor response for NO_2 exposure for a series of NO_2 pulses with concentrations ranging from 1 to 100 ppm for the pristine and decorated SnO disk-like structures performed at 250 °C. (b) Maximum sensor response measured for 100 ppm NO_2 exposure, in each working temperature for the pristine and decorated SnO disk-like structures.

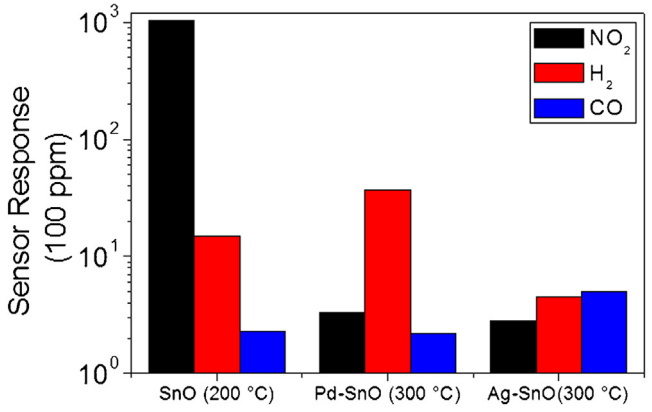

Fig. 8. Sensor response to 100 ppm of NO_2, H_2 and CO gases for pristine (at 200 °C working temperature), Pd-decorated (at 300 °C working temperature) and Ag-decorated (at 300 °C working temperature) SnO disk-like structures.

measurements were performed on both pristine and decorated SnO structures under simulated gas sensor operation conditions. Fig. 9 presents the results of IS measurements at the working temperature at which each sample exhibited its highest sensor response. An ideal single semicircle with its origin on the Z′ axis can be represented by a single resistor R in parallel with a single capacitor C as, for example, observed by the red curve (Pd-SnO) in the inset of Fig. 9a. Such circuits are described as having a single time constant $\tau = RC$. Depressed semicircles, as observed, for example, in the blue curve (Ag-SnO) in Fig. 9d, reflect the fact that there is an inhomogeneity in the process and that the response needs to be described in terms of circuits with a distribution of time constants. Two semicircles in series, as observed for the blue curve (Ag-SnO) in Fig. 9f, reflects the fact that the electrical response is representative of the two parallel RC circuits in series, with the one at lower frequencies having the larger time constant. This can be the case, for instance, in which the equivalent circuit represents contributions from the bulk (high frequency semicircle) and from the contact interface or electrodes (low frequency semicircle). In the following, we examine the changes induced in the impedance measurements of both the pristine and decorated SnO structures as a result of changes in gas composition and attempt to relate these changes to the location of the controlling reactions at the gas/solid interfaces.

The Nyquist plot for the pristine and the Ag- and Pd-decorated SnO materials are shown in Fig. 9. In air atmosphere, the Ag-decorated SnO structures have by far the highest impedance values at all measured temperatures. The initiation of a second semicircle at lower frequencies is evident for Ag-SnO disks, most clearly seen in Fig. 9c, which is likely related to a process at the interface of the disks. The orders of magnitude higher resistance of Ag-decorated SnO sample is consistent with the electronic sensitization model, wherein it is proposed that Ag-decorated structures exhibit electron-depleted zones induced by Ag/Ag^+ oxidation. The Pd sensitized sample, with an approximately five-fold increase in resistance over the unsensitized specimen can also be attributed to the formation of a Schottky barrier and consequent depletion of electrons in vicinity of the semiconductor-metal junction, but with lower barrier.

Fig. 9d shows the results for IS measurements performed instead with 20 ppm NO_2 at 200 °C. As adsorbed NO_2 molecules remove free electrons from the surface, the resistivity of all the materials increase, but the relative changes depend on each material's sensor response. As the pristine structures were found to be most sensitive to the NO_2 gas (see Fig. 7), it was expected that we would find a larger change in its resistance than for the sensitized specimens, which was confirmed. The pristine disk device resistance increased from 8.0×10^3 to 3.3×10^6 ohms. Interestingly, the Pd sensitized specimen showed the weakest sensor response to NO_2 increasing in resistance form 4.4×10^4 to 1.0×10^5 ohms (see Fig. 9d inset).

Fig. 9f presents the results upon exposure to 20 ppm H_2 at 300 °C. Under these conditions, the resistance of all materials decreased (due to the introduction of electrons promoted by H_2 oxidation), with the Pd-decorated SnO structure being less resistive than the pristine one. The Ag-decorated SnO structures exhibited two distinguishable semicircles, indicating the presence of two relaxation process, while the pristine and Pd-decorated structures appear to exhibit only one. This points to the fact that while the resistance changes in the undecorated and Pd decorated specimens are largely due to the change in the contact resistance of the SnO micro-disks, for the Ag-decorated specimens, an additional interfacial process is contributing to the overall impedance, generating a more complex electrical response. This points to an additional electron blocking activity at either the electrodes or at the interface between the micro-disks. Since the electrode material is the same in all cases, it points to the particle-disk interface as the main source of the additional impedance. This is perhaps not surprising given the role of electronic sensitization introduced by Ag nanoparticles, leading to enhanced charge depletion at the Ag/SnO interface. Given that the low frequency "semicircle" is nearly 4 times larger than the high frequency semicircle for the Ag-decorated specimen as measured in H_2 at 300 °C, this points to the fact that nearly 80% of the response to H_2 exhibited by this material is not related to a SnO–SnO resistance, but rather a modulation of the interface resistance between micro-disks and Ag particles. This is in strong contrast to that observed

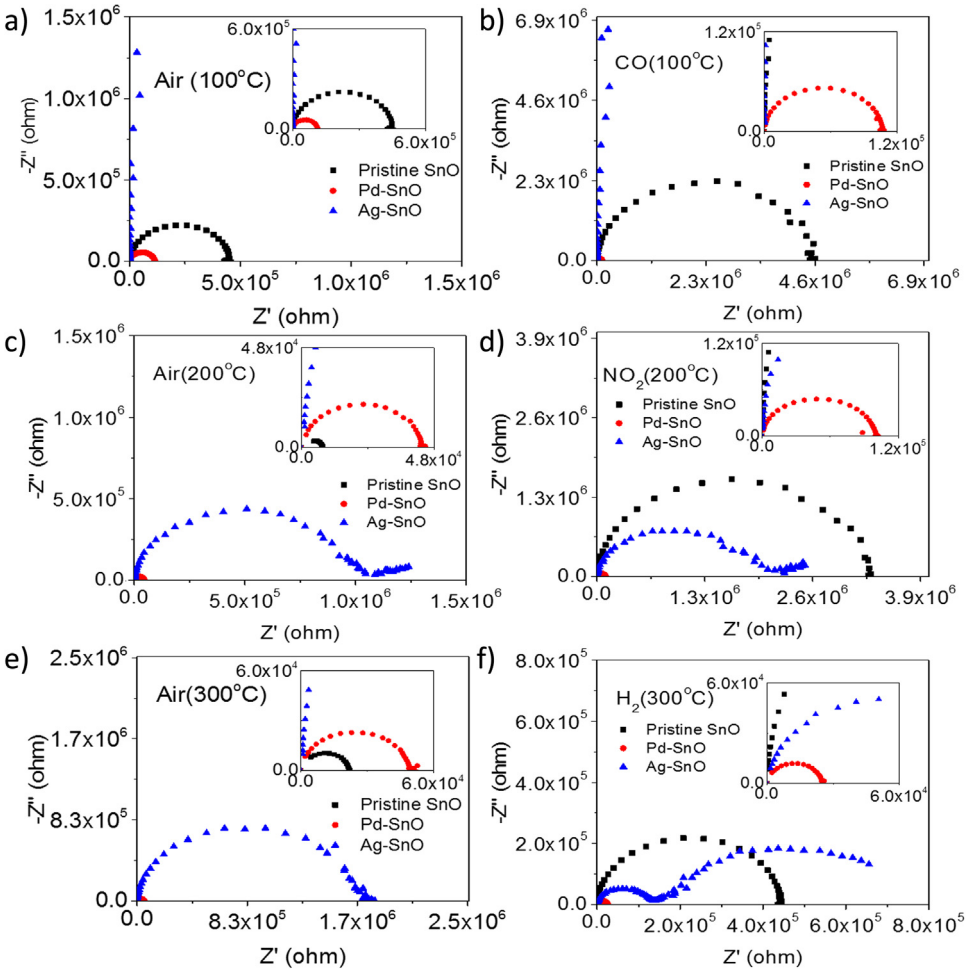

Fig. 9. IS characterization for the pristine and decorated SnO disk-like structures in different atmospheres and working temperatures: Synthetic dry air at (a) 100 °C, (c) 200 °C and (e) 300 °C; (b) 20 ppm CO at 100 °C, (d) 20 ppm NO_2 at 200 °C and (f) 20 ppm H_2 at 300 °C. (For interpretation of the references to colour in the text legend, the reader is referred to the web version of this article.)

for both undecorated and Pd-decorated specimens that show only the contact between disks effect. Thus aside from the higher sensor response of the Pd- vs the Ag-decorated SnO micro-disks to H_2, the simpler nature of the response of the Pd-decorated specimens could be expected to lead to longer-term stability of the sensor device.

4. Conclusions

SnO micro-disks decorated by catalytically active nanoparticles of Pd and Ag were shown to exhibit high sensor response to reducing gases as exemplified by H_2 and CO. On the other hand, they were observed to reduce the sensor response to oxidizing gases such as NO_2. These findings provide guidance on how to achieve both high sensor response and selectivity as illustrated in Figs. 5–7. The catalytic activity of Pd was found to be related to chemical sensitization unlike that of Ag that appears to be related to electronic sensitization. The former correlates with the well-known ability of Pd to support the H_2 to 2H *split-over* conversion followed by *spillover*. In contrast, both changes in conductivity on Ag-decorated structures, and their behavior when exposed to oxidizing and reducing gases, can be correlated to silver oxidation and reduction (Ag^0/Ag^+ equilibria) leading to electron-depleted regions. The application of impedance spectroscopy enabled deconvolution of different contributions to the sensor response. Only Ag-decorated specimens exhibited two *semicircles* response, corresponding to two different time constants. This showed that in contrast to undecorated and Pd-decorated specimens, nearly 80% of the Ag decorated sensors' response to H_2 was controlled by changes in the interfacial resistance between Ag particles and disks, leading perhaps ultimately to a less stable device. Optimum temperature of operation changed according to each gas, as the result of the diverse gas-solid interaction mechanisms. Sensor response to H_2 being related to the reaction with O_2 species, were optimal at higher temperatures (300 °C). In the case of NO_2 (direct interaction with electron pairs), the maximum sensor response was observed at 200 °C. For Pd-decorated materials, CO sensor response was enhanced at lower temperatures (under 150 °C), where CO absorption by metal nanoparticles is favored.

Acknowledgements

The authors acknowledge the São Paulo Research Foundation (FAPESP) (Procs. 2012/51195-3, 2013/08734-3, 2013/18511-1 and 2014/50725-4) for financial support to the international MIT/BRAZIL collaboration and CNPq for general research funding (# 447760/2014-9). TEM and FEG-SEM facilities were provided by the IQ-UNESP. XPS analysis was performed at LEFE/IQ-UNESP. HLT thanks the MIT International Science and Technology Initiatives (MISTI) MIT-Brazil Program for travel to São Paulo State University as part of our collaboration. This work was also supported in part by the MRSEC Program of the National Science Foundation under award number DMR – 141980.

Appendix A. Supplementary data

Supplementary data associated with this article can be found, in the online version, at http://dx.doi.org/10.1016/j.snb.2016.07.157.

References

[1] I.-D. Kim, A. Rothschild, H.L. Tuller, Advances and new directions in gas-sensing devices, Acta Mater. 61 (2013) 974–1000.
[2] N.S. Ramgir, Y. Yang, M. Zacharias, Nanowire-based sensors, Small 6 (2010) 1705–1722.
[3] S. Matsushima, Y. Teraoka, N. Miura, N. Yamazoe, Electronic interaction between metal additives and tin dioxide in tin dioxide-based gas sensors, Jpn. J. Appl. Phys. 1 (27) (1988) 1798–1802.
[4] M.E. Franke, T.J. Koplin, U. Simon, Metal and metal oxide nanoparticles in chemiresistors: does the nanoscale matter, Small 2 (2006) 36–50.
[5] S.-W. Choi, A. Katoch, G.-J. Sun, P. Wu, S.S. Kim, NO_2-sensing performance of SnO_2 microrods by functionalization of Ag nanoparticles, J. Mater. Chem. C 1 (2013) 2834–2841.
[6] H.-Y. Lai, C.-H. Chen, Highly sensitive room-temperature CO gas sensors: Pt and Pd nanoparticle-decorated In_2O_3 flower-like nanobundles, J. Mater. Chem. C 22 (2012) 13204–13208.
[7] C.-M. Chang, M.-H. Hon, I.-C. Leu, Improvement in CO sensing characteristics by decorating ZnO nanorod arrays with Pd nanoparticles and the related mechanisms, RSC Adv. 2 (2012) 2469–2475.
[8] M. Schweizer-Berberich, J.G. Zheng, U. Weimar, W. Gopel, N. Barsan, E. Pentia, A. Tomescu, The effect of Pt and Pd surface doping on the response of nanocrystalline tin dioxide gas sensors to CO, Sens. Actuators B 31 (1996) 71–75.
[9] G. Korotcenkov, Gas response control through structural and chemical modification of metal oxide films: state of the art and approaches, Sens. Actuators B 107 (2005) 209–232.
[10] J.F. McAleer, P.T. Moseley, J.O.W. Norris, D.E. Williams, B.C. Tofield, Tin dioxide gas sensors—Part 2: the role of surface additives, J. Chem. Soc. Faraday Trans. 1 84 (1988) 441–457.
[11] P.H. Suman, A.A. Felix, H.L. Tuller, J.A. Varela, M.O. Orlandi, Giant chemo-resistance of SnO disk-like structures, Sens. Actuators B 186 (2013) 103–108.
[12] P.H. Suman, A.A. Felix, H.L. Tuller, J.A. Varela, M.O. Orlandi, Comparative gas sensor response of SnO_2, SnO and Sn_3O_4 nanobelts to NO_2 and potential interferents, Sens. Actuators B 208 (2015) 122–127.
[13] M.O. Orlandi, A.J. Ramirez, E.R. Leite, E. Longo, Morphological evolution of tin oxide nanobelts after phase transition, Cryst. Growth Des. 8 (2008) 1067–1072.
[14] P.H. Suman, M.O. Orlandi, Influence of processing parameters on nanomaterials synthesis efficiency by a carbothermal reduction process, J. Nanopart. Res. 13 (2011) 2081–2088.
[15] F. Fievet, J.P. Lagier, B. Blin, B. Beaudoin, M. Figlarz, Homogeneous and heterogeneous nucleations in the polyol process for the preparation of micron and sub-micron size metal particles, Solid State Ionics 32–33 (1989) 198–205.
[16] L.J. Chen, C.C. Wan, Y.Y. Wang, Chemical preparation of Pd nanoparticles in room temperature ethylene glycol system and its application to electroless copper deposition, J. Colloid Interface Sci. 297 (2006) 143–150.
[17] B. Wiley, T. Herricks, Y.G. Sun, Y.N. Xia, Polyol synthesis of silver nanoparticles: use of chloride and oxygen to promote the formation of single-crystal, truncated cubes and tetrahedrons, Nano Lett. 4 (2004) 1733–1739.
[18] Y. Zhang, Q. Xiang, J.Q. Xu, P.C. Xu, Q.Y. Pan, F. Li, Self-assemblies of Pd nanoparticles on the surfaces of single crystal ZnO nanowires for chemical sensors with enhanced performances, J. Mater. Chem. 19 (2009) 4701–4706.
[19] J.M. Themlin, M. Chtaib, L. Henrard, P. Lambin, J. Darville, J.M. Gilles, Characterization of tin oxides by x-ray-photoemission spectroscopy, Phys. Rev. B 46 (1992) 2460–2466.
[20] G. Polzonetti, M.V. Russo, G. Infante, A. Furlani, The interface between aluminium and a rod-like organometallic Pd-containing polymer film investigated by XPS, J. Electron Spectrosc. Relat. Phenom. 85 (1997) 73–80.
[21] I.-S. Hwang, J.-K. Choi, H.-S. Woo, S.-J. Kim, S.-Y. Jung, T.-Y. Seong, I.-D. Kim, J.-H. Lee, Facile control of C_2H_5OH sensing characteristics by decorating discrete Ag nanoclusters on SnO_2 nanowire networks, ACS Appl. Mater. Interfaces 3 (2011) 3140–3145.
[22] U. Roland, F. Roessner, A new model on the nature of spilt-over hydrogen, Stud. Surf. Sci. Catal. 112 (1997) 191–200.
[23] T.B. Fryberger, S. Semancik, Conductance response of Pd/SnO_2 (110) model gas sensors to H_2 and O_2, Sens. Actuators B 2 (1990) 305–309.
[24] G. Martinelli, M.C. Carotta, Thick-film gas sensors, Sens. Actuators B 23 (1995) 157–161.
[25] N. Yamazoe, Y. Kurokawa, T. Seiyama, Effects of additives on semiconductor gas sensors, Sens. Actuators 4 (1983) 283–289.
[26] Y. Ogo, H. Hiramatsu, K. Nomura, H. Yanagi, T. Kamiya, M. Kimura, M. Hirano, H. Hosono, Tin monoxide as an s-orbital-based p-type oxide semiconductor: electronic structures and TFT application, Phys. Status Solidi A 206 (2009) 2187–2191.
[27] G.W. Smith, E.A. Carter, Interactions of NO and CO with Pd and Pt atoms, J. Phys. Chem. 95 (1991) 2327–2339.
[28] D.D. Trung, N.D. Hoa, P. Van Tong, N. Van Duy, T.D. Dao, H.V. Chung, T. Nagao, N. Van Hieu, Effective decoration of Pd nanoparticles on the surface of SnO_2 nanowires for enhancement of CO gas-sensing performance, J. Harazad. Mater. 265 (2014) 124–132.
[29] K. Veltruska, N. Tsud, V. Brinzari, G. Korotchenkov, V. Matolin, CO adsorption on Pd clusters deposited on pyrolytically prepared SnO_2 studied by XPS, Vacuum 61 (2001) 129–134.
[30] W.K. Kuhn, J. Szanyi, D.W. Goodman, CO adsorption on Pd (111): the effects of temperature and pressure, Surf. Sci. 274 (1992) L611–L618.
[31] G. Korotcenkov, B.K. Cho, L.B. Gulina, V.P. Tolstoy, Gas sensing properties of SnO_2 thin films modified by Ag nanoclusters synthesized by SILD method, Proc. World Acad. Sci. Eng. Technol. 81 (2011) 199–202.
[32] D.-J. Yang, I. Kamienchick, D.Y. Youn, A. Rothschild, I.-D. Kim, Ultrasensitive and highly selective gas sensors based on electrospun SnO_2 nanofibers modified by Pd loading, Adv. Funct. Mater. 20 (2010) 4258–4264.

Biographies

Martin S. Barbosa received his degree in chemistry from São Paulo State University in 2012 and his master's degree in chemistry from São Paulo State University in 2015. His research interests are synthesis and electrochemistry of nanostructured semiconductor materials for sensor applications. He is currently a PhD student in the Chemistry program at Sao Paulo state university, under the supervision of Professor Dr. Marcelo Orlandi.

Pedro H. Suman received his degree in Physics from São Paulo State University (2009) and his Master degree in Materials Science and Technology also from São Paulo State University (2012). He worked in collaboration with Prof. Tuller's group as a PhD visiting student in the Department of Materials Science and Engineering at MIT. Currently, Pedro is a PhD student at São Paulo State University under supervision of Prof. Marcelo O. Orlandi. His research interest is mainly about the synthesis of pure and hybrid semiconductor nanomaterials for chemical sensor applications.

Jae Jin Kim received his B.S. (2006) and M.S. (2008) degrees from Seoul National University and Ph.D. (2015) degree from MIT, all in Materials Science and Engineering. He is currently a postdoctoral researcher in the Chemical Sciences and Engineering at Argonne National Laboratory, where he conducts research on electrochemical energy storage technologies at the Molecular-scale science department. His research emphasizes in situ characterization of solid/gas and solid/liquid interfaces in model battery and fuel cell structures.

Harry L. Tuller is a Professor of Ceramics and Electronic Materials; Department of Materials Science and Engineering and Head of the Crystal Physics and Electroceramics Laboratory at MIT. He received B.S. and M.S. degrees in Electrical Engineering and Eng.Sc.D. in Solid State Science & Engineering from Columbia University, NY; served as Postdoctoral Research Associate; Physics, Technion, Israel, following which he joined the faculty at MIT. His research focuses on defects, diffusion, and the electrical, electrochemical and optical properties of metal oxides with applications to sensors, fuel cells and photoelectrochemistry. He has published over 435 articles, co-edited 15 books and was awarded 33 patents.

José A. Varela is graduated in Physics from University of São Paulo (1968), and received his Master Degree in Physics from Technological Institute of Aeronautics (1975) both in Brazil. He received PhD in Materials Science from University of Washington, Seattle, WA, USA in 1981. He has been Professor at University of São Paulo State – UNESP, Brazil since 1983. His main research interests are microwave assisted hydrothermal synthesis of inorganic materials as well as ceramic thin films chemical and physical deposition for applications including ferroelectrics, varistors, electro-optical and sensors. Prof. Varela passed away on May, 17, 2016.

Marcelo O. Orlandi is physicist with PhD in Material Science and Engineering field by Federal University of São Carlos (2005) having a professor position at São Paulo State University since 2006. In the last few years the main focus of Dr. Orlandi research has been the controllable growth and modeling of nanomaterials and the sensor response of nanomaterials. Other areas of interest are transport in nanomaterials and electron microscopy.